Applied Surface Science 441 (2018) 841–852

Contents lists available at ScienceDirect

Applied Surface Science

journal homepage: www.elsevier.com/locate/apsusc

Full Length Article

Reversible switching of wetting properties and erasable patterning of polymer surfaces using plasma oxidation and thermal treatment

Zeeshan Rashid [a], Ipek Atay [b], Seren Soydan [c], M. Baris Yagci [d], Alexandr Jonáš [e], Emel Yilgor [b,d], Alper Kiraz [a,d,f,*], Iskender Yilgor [b,d,*]

[a] Department of Electrical and Electronics Engineering, Koç University, 34450 Sariyer, Istanbul, Turkey
[b] Department of Chemistry, Koç University, 34450 Sariyer, Istanbul, Turkey
[c] Department of Physics, Istanbul Technical University, 34469 Maslak, Istanbul, Turkey
[d] Koç University Surface Science and Technology Center (KUYTAM), Rumeli Feneri Yolu, 34450 Sariyer, Istanbul, Turkey
[e] Institute of Scientific Instruments of the CAS, v.v.i., The Czech Academy of Sciences, Královopolská 147, 612 64 Brno, Czech Republic
[f] Department of Physics, Koç University, 34450 Sariyer, Istanbul, Turkey

ARTICLE INFO

Article history:
Received 1 November 2017
Revised 25 January 2018
Accepted 8 February 2018
Available online 9 February 2018

Keywords:
Reversible wetting
Plasma oxidation
Superhydrophobic
Superhydrophilic

ABSTRACT

Polymer surfaces reversibly switchable from superhydrophobic to superhydrophilic by exposure to oxygen plasma and subsequent thermal treatment are demonstrated. Two inherently different polymers, hydrophobic segmented polydimethylsiloxane-urea copolymer (TPSC) and hydrophilic poly(methyl methacrylate) (PMMA) are modified with fumed silica nanoparticles to prepare superhydrophobic surfaces with roughness on nanometer to micrometer scale. Smooth TPSC and PMMA surfaces are also used as control samples. Regardless of their chemical structure and surface topography, all surfaces display completely reversible wetting behavior changing from hydrophobic to hydrophilic and back for many cycles upon plasma oxidation followed by thermal annealing. Influence of plasma power, plasma exposure time, annealing temperature and annealing time on the wetting behavior of polymeric surfaces are investigated. Surface compositions, textures and topographies are characterized by X-ray photoelectron spectroscopy (XPS), scanning electron microscopy (SEM) and white light interferometry (WLI), before and after oxidation and thermal annealing. Wetting properties of the surfaces are determined by measuring their static, advancing and receding water contact angle. We conclude that the chemical structure and surface topography of the polymers play a relatively minor role in reversible wetting behavior, where the essential factors are surface oxidation and migration of polymer molecules to the surface upon thermal annealing. Reconfigurable water channels on polymer surfaces are produced by plasma treatment using a mask and thermal annealing cycles. Such patterned reconfigurable hydrophilic regions can find use in surface microfluidics and optofluidics applications.

1. Introduction

Smart surfaces with wettability tunable between superhydrophobic and superhydrophilic regimes have received widespread scientific attention in the last two decades due to their potential applications in industry and basic research [1]. Apart from daily life applications such as anti-fogging, anti-reflection and self-cleaning, reconfigurable surfaces provide a simple platform for droplet manipulations, directed motility of biological cells, chemical reagent delivery, biosensing and rewritable surface microfluidics [2]. Furthermore, advancements with respect to ease and flexibility in microfluidic manipulation require the development of reconfigurable surfaces which can be controlled quickly and efficiently and which can operate reliably over several cycles of wetting transitions.

Reversible switching of surface wetting properties can be achieved by various approaches such as temperature change [3], solvent treatment [4], pH change [1], adjustment of electric potential [5], light irradiation [6] and plasma exposure [7]. Among these, light and plasma treatments are especially convenient since they are dry processes offering non-contact exposure free of contamination, and enable low temperature surface processing without altering the bulk properties of the polymers [8]. In addition, they allow for selective, localized change in surface wetting properties by the use of simple masks [9]. A large number of stimuli responsive polymeric surfaces have been developed in recent years with the major

* Corresponding authors at: Koç University Surface Science and Technology Center (KUYTAM), Rumeli Feneri Yolu, 34450 Sariyer Istanbul, Turkey.
E-mail addresses: akiraz@ku.edu.tr (A. Kiraz), iyilgor@ku.edu.tr (I. Yilgor).

https://doi.org/10.1016/j.apsusc.2018.02.089
0169-4332/

focus on simplifying the transition process, increasing the number of switching cycles and enhancing the wetting contrast between the two states [1,2,7]. It is expected that changes in wettability can be increased in both directions (hydrophobic and hydrophilic) after introducing roughness in the wetted surface by stimuli responsive nanoparticles [10,6].

Over the past few years, numerous studies have been reported on the fabrication of surfaces that switch their wetting behavior from superhydrophobic to superhydrophilic when triggered with ultraviolet (UV) radiation. Lim et al. developed (silica/polyallylamine hydrochloride) (SiO_2/PAH) surfaces modified with fluorinated azobenzene, which displayed switchable superhydrophobicity with erasable and rewritable patterns upon UV/visible light irradiation causing reversible photoisomerization of fluorinated azobenzene [6]. To this end, the surface layer was coated with fluorinated azobenzene after silanization, which provided binding sites for photoswitchable moieties. The contact angle contrast was then investigated as a function of the number of layers deposited by layer-by-layer coating technique which introduced higher roughness to the film surface. After nine deposition cycles of SiO_2/PAH, the contact angle of water droplet was observed to change from 152° to 5° after 20 min of UV irradiation (λ = 365 nm) and back to 152° by 3 h of visible irradiation (λ = 440 nm). Sun et al. fabricated poly(styrene-n-butyl acrylate-acrylic acid) films mixed with photoresponsive TiO_2 nanoparticles [1]. After UV illumination at 150 W for 2 h, the contact angle of water droplets changed from 156° to 0°; original superhydrophobicity was then recovered after annealing at 150 °C for 1 h. In addition to UV exposure, the same film was also demonstrated to switch from superhydrophobic to superhydrophilic wetting characteristics as a function of pH. The as-obtained film was treated with NaOH solution (pH = 12), which caused deprotonation of covalently bonded COOH group to ionic and highly hydrophilic COO^-Na^+ groups. After dipping the NaOH treated film in HCl solution (pH = 2), COO^- groups were reverted to COOH groups. Petroffe et al. achieved fast reversible switching of contact angle between 118° and 18°, which was achieved by 12 min of UV exposure followed by annealing at 150 °C for 20 min [2]. To this end, they used photosensitive TiO_2 nanoparticles mixed in 11-(4-phenylazo)phenoxy undecanoic acid.

In spite of the simplicity of light activated switchable surfaces explored in recent years, UV induced chemical reactions that change wettability from superhydrophobic to superhydrophilic are slow even with the use of high power lamps. In contrast, oxygen plasma allows abrupt chemical modification by tuning gas phase chemistry and ion bombardment energy. Extremely short and highly reactive exposure of the target surface is of paramount importance because it ensures maximum modification of chemical structure and minimum physical or topographical change or damage. Any irreversible physical alteration in the surface topography limits the performance of the exposed surfaces in terms of absolute recovery and count of useful switching cycles even if the surface returns to its original chemical state. Tsougeni et al. performed comprehensive analysis of poly(methyl methacrylate) (PMMA) and poly(ether ether ketone) (PEEK) surfaces using scanning electron microscopy (SEM) and X-ray photoelectron spectroscopy (XPS) at different plasma powers and exposure times to investigate self-recovery of hydrophobicity, roughness and chemical composition under ambient conditions, which they termed as aging [8]. Depending on the duration of the oxygen plasma treatment, recovery time for PEEK surfaces from superhydrophilic to superhydrophobic varied between 140 and 240 days. PMMA surfaces were only able to reach a contact angle value of 70° after 120 days of annealing at room temperature and never recovered to become superhydrophobic. Xue et al. prepared reconfigurable surfaces by spraying polystyrene/silica (PS/SiO_2) core/shell nanoparticles as a base and polydimethylsiloxane (PDMS) as the hydrophobic coating [7]. After plasma treatment, obtained hydrophilic surfaces could be switched to the original hydrophobic state in 12 h at room temperature or by heating to 150 °C for 1 h and treatment with tetrahydrofuran, which is a good solvent for PS. Thermal treatment at 150 °C was the most efficient recovery method but it could only provide three full switching cycles; in the fourth cycle, thermal annealing of the hydrophilic surface only provided the contact angle recovery of 40°.

Numerous methods have been reported for the preparation of superhydrophobic polymer surfaces; these include; phase separation [11], physical or chemical etching [12,13], electrospinning [14], UV or X-ray lithography [15,16], templating [17], sol-gel processing [18], layer-by-layer deposition [18,19,16], various wet coating techniques [16,19–22] and many others [12,23–26]. Some of these processes are rather complex, some need specialized equipment and more critically, some approaches are polymer specific. It is well established that a simple method for the preparation of superhydrophobic polymer surfaces is through incorporation of various hydrophobically coated inorganic oxide nanoparticles, such as TiO_2, SiO_2 and ZnO, at a specific concentration [2]. Despite this, only a limited number of reports are available in the literature on the evaluation of switchability of these surfaces from superhydrophobic to superhydrophilic and back by plasma and subsequent thermal treatment.

Light and plasma treatment can be combined with masks in order to obtain patterned fluidic channels for surface microfluidics and optofluidics applications. Hong et al. demonstrated droplet transport along structured surfaces fabricated by a single step lithographic process using superhydrophobic photosensitive nanocomposite formula [27]. In particular, they used photopatternable superhydrophobic nanocomposite (PSN) which incorporates polytetrafluoroethylene (PTFE) nanoparticles into SU-8 (negative photoresist) polymer matrix. PTFE nanoparticles contributed to surface roughness required for superhydrophobicity and SU-8 provided photopatternability and adhesion to glass substrate. Hydrophilic glass surface having water contact angle of 10° was used as a route for liquid transport which was surrounded by superhydrophobic nanocomposite region. Xing et al. performed transport of aqueous droplets along hydrophilic patterns fabricated using two-step laser micromachining [28]. In the first step, they treated PDMS coating deposited on a glass substrate with a scanned CO_2 pulsed laser beam at optimized power and scanning speed and obtained extremely porous nanostructures with high water contact angles. In the second step, they locally removed the previously prepared nanostructured superhydrophobic PDMS layer following the target pattern again by the same laser beam but at different operating conditions to expose the underlying hydrophilic glass. Both techniques reported above are irreversible in nature; moreover, apart from generating contrast of wetting properties they also produced a topographic feature (a shallow hydrophilic channel) which provides additional liquid confinement.

In this study, we prepared superhydrophobic surfaces based on hydrophilic PMMA and hydrophobic segmented polydimethylsiloxane-urea copolymer (TPSC) by incorporation of hydrophobic fumed silica particles into polymer layers deposited on supporting glass substrates [29]. Surfaces obtained in this way could be converted to superhydrophilic upon oxygen plasma exposure and back to superhydrophobic by thermal annealing for six cycles. We also compared the recovery of hydrophobicity of unmodified, smooth polymer surfaces that served as control samples. In order to correlate the change in the wetting behavior to surface chemistry and topography, all surfaces were characterized by XPS, SEM and white light interferometry (WLI).

In addition to modifying the wetting properties of the target surfaces, we also extended our approach to the preparation of erasable and rewritable hydrophilic channels surrounded by bulk

hydrophobic areas for controlled liquid transport in surface microfluidic applications. With this simple approach, filaments of polar liquids can be guided along hydrophilic channels without any physical or structural support. We generated the patterns of surface wettability by using a 1 mm thick PDMS mask with good adhesion to TPSC-coated surfaces. The mask with narrow openings was sealed over the TPSC-coated substrate, allowing plasma to react only with the exposed region. The mask thickness of 1 mm was found to be sufficient to protect the covered surface regions from the effects of reactive oxygen species. Schematic diagram illustrating this process for the production of rewritable hydrophilic channels is shown in Fig. 1. Such surfaces can be used to obtain reconfigurable fluidic channels, optofluidic waveguides, and droplet guiding tracks for applications in surface microfluidics [27,28], optofluidics [30], and droplet microfluidics [31,32].

2. Experimental

2.1. Materials

TPSC (Geniomer TPSC 140) with PDMS content of about 92% by weight and hydrophobic fumed silica, H2000 (HDK) were kindly provided by Wacker Chemie, Munich, Germany. Primary particle size and specific surface area of the hydrophobic silica were reported to be 5–30 nm and 170–230 m^2/g respectively. PMMA (M_n = 190,000 g/mol) was synthesized in our laboratories. Reagent grade isopropanol (IPA), tetrahydrofuran (THF) and toluene were obtained from Merck and used as received.

2.2. Preparation of polymeric coatings

PMMA and TPSC solutions were prepared at a concentration of 0.5% by weight in toluene and IPA respectively, by stirring overnight with a magnetic stirrer. HDK was added into these solutions to the final polymer/silica ratio of 1/10 by weight. Polymer/silica mixtures were further stirred for 30 min followed by sonication at a frequency of 35 kHz for 10 h to obtain homogeneous dispersions. Glass slides (20 × 20 × 0.15 mm), which were used as substrates were cleaned by wiping with IPA and THF several times. Subsequently, PMMA and TPSC solutions and PMMA/HDK and TPSC/HDK dispersions were spin-coated on clean glass slides at 1000 rpm for 70 s to obtain films with an average thickness of 20 to 30 μm using Model 7600 Spin Coater by Specialty Coating Systems, Inc., Indianapolis, IN, USA. Samples were first dried in a hood overnight and then in a vacuum oven at room temperature for 24 h.

2.3. Oxygen plasma treatment and thermal treatment

Polymeric films were oxidized in an oxygen plasma generator (Euro plasma SN 010/226) operating at a base pressure of 500 mT and 1 W power for 10 s. After oxidation, water contact angles were determined. Subsequently, the films were transferred into a constant-temperature vacuum oven to recover back their original hydrophobic state. For each full treatment cycle, virgin PMMA and TPSC samples were annealed in a 100 °C oven for 20 min, whereas superhydrophobic TPSC and PMMA samples were annealed in a 150 °C oven for 1 h.

2.4. Surface characterization techniques

Contact angle measurements were performed by placing 5 μL droplets of deionized water on the film surface. Snapshots of droplets were captured and stored using a CMOS camera (Thorlabs; DCC1545M) and a matched achromatic doublet pair (Thorlabs; MAP10100100-A-1:1, Magnification: 1) placed between the sample and the camera such that both the sample and the camera were at the foci of the two lenses forming the pair. The sample was illuminated from the direction opposite to the lens/camera location. The contact angle of the droplets from each recorded snapshot was measured by ImageJ software with a Drop Snake plug in [33]. At least five contact angle measurements were made on each sample surface and their average and standard deviation were used to characterize the surfaces.

Surface images of polymer layers deposited on the substrates were obtained at each step of the process by Field Emission Scanning Electron Microscope (FESEM) (Zeiss Ultra Plus) operating at 2–10 kV. To minimize surface charging, all sample surfaces were sputtered by 10 nm of gold prior to SEM investigation. Furthermore, topographies of virgin polymer surfaces and polymer-silica composite surfaces coated with 50 nm gold films were examined by WLI mounted on a Bruker Contour GT Motion 3D Microscope and Non-Contact Surface Profiler in the vertical scanning interferometry (VSI) mode. Using WLI, it is possible to measure feature sizes from sub nanometer to millimeter range [34]. In VSI mode, average surface roughness of the samples with height discontinuities ranging between 150 nm to several mm can be precisely measured. In our studies, 10 surface maps with dimensions of 126 × 94 μm^2 were obtained from different sections of the silica-coated samples to determine the values of the average surface roughness.

Chemical compositions of sample surfaces were investigated using XPS (Thermo Scientific K-Alpha X-ray) equipped with an aluminum anode (Al Kα = 1468.3 eV) at 90° electron take-off angle (between the film surface and the axis of the analyzer lens). Pass energy of 50 eV and energy step of 0.1 eV were set to acquire the data. A flood gun was employed to reduce surface charging. Spectra were recorded and processed using Avantage 5.9 software. All C1s peaks corresponding to hydrocarbons were calibrated at a binding energy of 284.5 eV (FWHM = 1.5 eV) to correct for the energy shift caused by surface charging.

3. Results and discussion

In this section, we demonstrate preparation and characterization of polymer-based surfaces reversibly switchable from

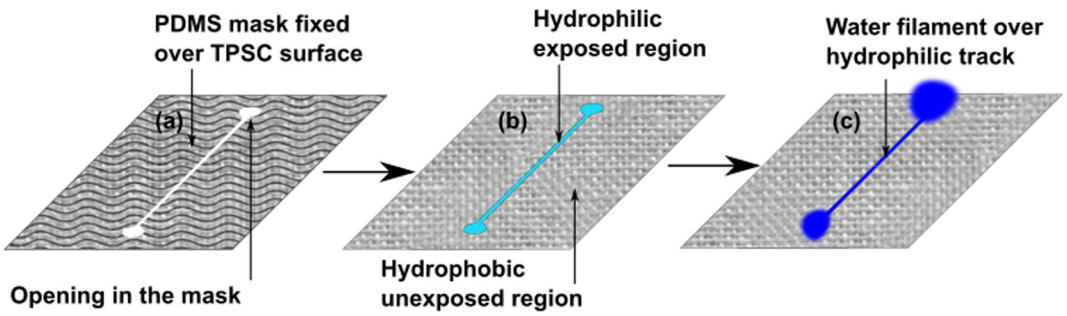

Fig. 1. Schematic representation of the processes used for the preparation of rewritable hydrophilic channels.

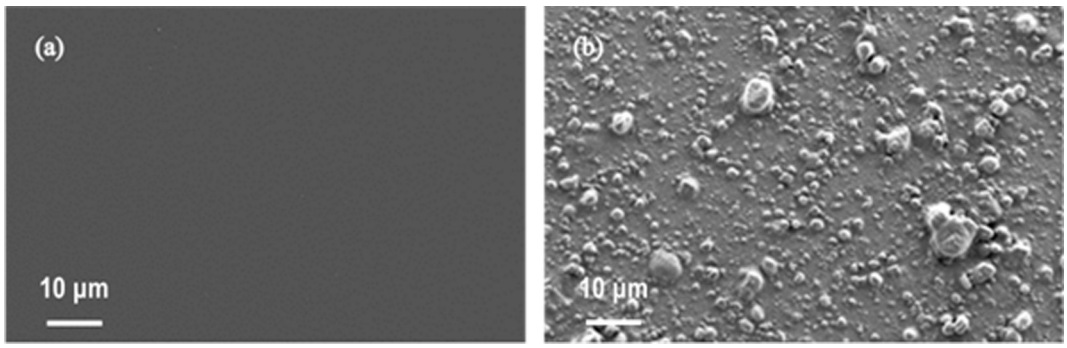

Fig. 2. SEM images of (a) virgin PMMA and (b) superhydrophobic PMMA.

Table 1
Values of average surface roughness (R_a), static, advancing and receding water contact angles (CA) and contact angle hysteresis (CAH) of investigated surfaces.

Sample	R_a (nm)	Static CA (°)	Adv. CA (°)	Rec. CA (°)	CAH (°)
PMMA	13.0 ± 5.2	67.5 ± 0.6	72.5 ± 1.5	52.5 ± 0.6	20.0
SHPMMA	250 ± 82	160.1 ± 0.5	162.2 ± 0.3	157.0 ± 2.8	5.2
TPSC	6.3 ± 1.0	110.3 ± 0.7	115.0 ± 1.0	93.6 ± 0.6	21.4
SHTPSC	125 ± 17	163.9 ± 0.6	166.7 ± 1.4	164.9 ± 1.2	1.8

superhydrophobic to superhydrophilic and back upon exposure to oxygen plasma followed by thermal annealing. We also investigate the influence of the chemical structure of the polymer, surface topography and annealing time on the wetting behavior of the studied surfaces. Four polymer surfaces considered in this study are hydrophilic PMMA, hydrophobic TPSC, superhydrophobic PMMA (SHPMMA) and superhydrophobic TPSC (SHTPSC). Superhydrophobic surfaces were obtained by modification of the host polymers with fumed silica as described in the experimental Section 2.2 [29]. SEM images of surfaces of fairly smooth and featureless PMMA and rough SHPMMA covered with micron sized, agglomerated silica particles are provided in Fig. 2 as general examples. Average surface roughness (R_a), static, advancing and receding water contact angles (CA) and contact angle hysteresis (CAH) values of all polymer surfaces investigated in this study are provided in Table 1.

As shown in Table 1, virgin PMMA and TPSC surfaces are extremely smooth with R_a values of 13 nm and 6.3 nm, respectively. On the contrary, SHPMMA and SHTPSC surfaces have an order of magnitude higher R_a values. Owing to their roughness, these surfaces display truly superhydrophobic behavior with average static water contact angles of 160.1° and 163.9°, respectively and very small contact angle hysteresis values of 5.2° and 1.8°, respectively.

3.1. Reversible switching of wetting properties of polymeric surfaces upon oxygen plasma treatment and thermal annealing

Images of water contact angles on smooth PMMA and TPSC surfaces after 10 s treatment with oxygen plasma at 1 W, followed by annealing at 100 °C for 20 min are provided in Fig. 3a and b, respectively. Slightly hydrophilic virgin PMMA surface, which displays a contact angle of 67.5 ± 0.6° before plasma exposure, becomes highly hydrophilic and displays an average water contact angle of 26 ± 3°. Upon annealing at 100 °C for 20 min, water contact angle increases back to the original value of 65 ± 3°. Fairly hydrophobic virgin TPSC surface with a water contact angle of 11 0.3 ± 0.7°, becomes hydrophilic upon plasma exposure and displays an average contact angle of 23 ± 2°. After annealing, the contact angle increases back to 100 ± 2°. These results clearly demonstrate reversible switching of wetting behavior of PMMA and TPSC surfaces, which can be repeated for many cycles as shown in Fig. 4.

For superhydrophobic polymeric surfaces containing fumed silica, the difference of water contact angles after plasma treatment and thermal annealing is much more dramatic. As can be seen in Fig. 5a and b, when SHPMMA and SHTPSC surfaces are treated with oxygen plasma at 1 W for 10 s, they both show instantaneous and complete wetting and, therefore, display truly superhydrophilic behavior. Upon annealing at 150 °C for 1 h, both surfaces recover nicely. Thermally annealed SHPMMA displays contact angles around 125° upon recovery, whereas SHTPSC displays much higher contact angles around 140°. As shown in Fig. 6, the surfaces can be reversibly switched between the two extremal wetting states for at least 6 cycles without any significant degradation of their wetting characteristics

3.1.1. Influence of annealing time on the recovery of surface hydrophobicity

Annealing temperature and time play critical roles in the recovery of hydrophobic character of the surface. After investigating var-

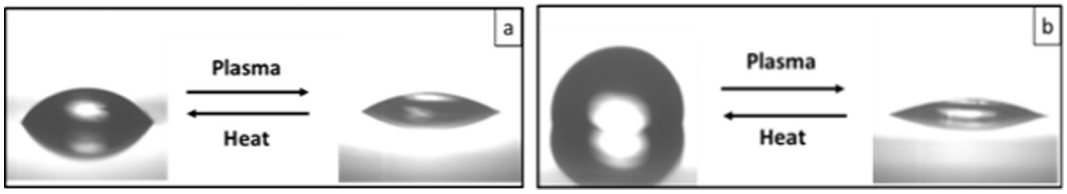

Fig. 3. Static water contact angles on (a) PMMA and (b) TPSC surfaces after oxygen plasma treatment (right part of the images) and thermal annealing (left part of the images).

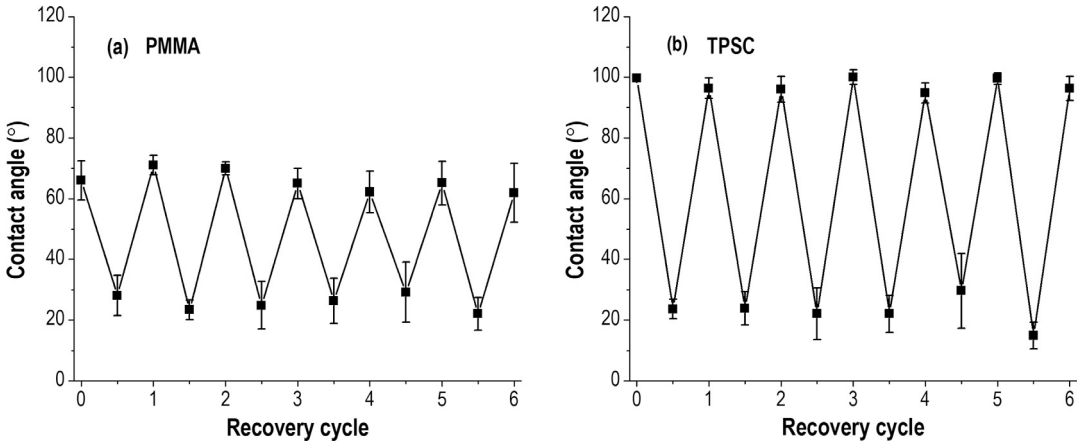

Fig. 4. Reversible switching of wetting properties of (a) PMMA and (b) TPSC surfaces upon cyclic exposure to oxygen plasma followed by thermal annealing.

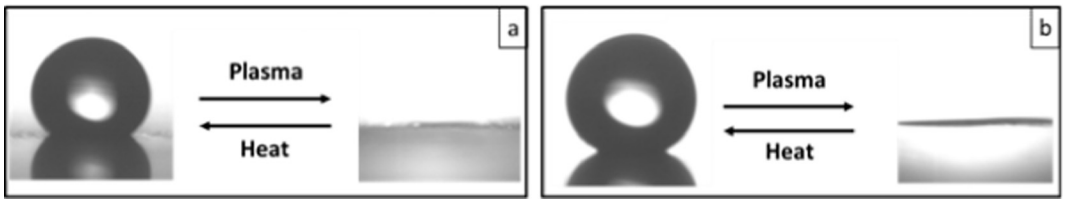

Fig. 5. Static water contact angles on (a) SHPMMA and (b) SHTPSC surfaces after oxygen plasma treatment (right part of the images) and thermal annealing (left part of the images).

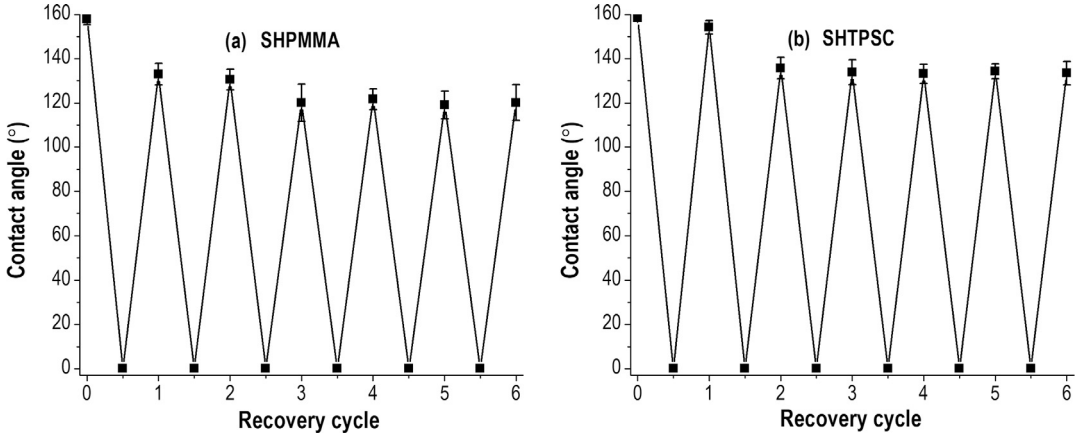

Fig. 6. Reversible switching of wetting properties of (a) SHPMMA and (b) SHTPSC surfaces upon cyclic exposure to oxygen plasma followed by thermal annealing.

ious annealing temperatures, we decided to use 100 °C for PMMA and TPSC samples and 150 °C for SHPMMA and SHTPSC samples. 100 °C is very close to the glass transition temperature of PMMA, which is 105 °C and also to the temperature where hydrogen bonding between urea linkages in TPSC starts weakening [35]. This allows the polymer chains to move fairly freely in the bulk and also at the surface for optimum recovery. For SH samples, annealing at a higher temperature for a longer time is required because of the restricted chain mobility of the polymer molecules due to interactions with the silica particles in the nanocomposites. After deciding on the annealing temperatures, influence of annealing time on the recovery of surface hydrophobicity was systematically studied. As expected and as shown in Fig. 7a, for TPSC and PMMA, contact angles increased with annealing time and reached to a plateau value after 20 min. On the other hand, for SHPMMA and SHTPSC, it took about 60 min to reach maximum contact angle recovery as shown in Fig. 7b.

3.2. Characterization of changes in the surface chemical composition upon plasma treatment/thermal annealing

Relative chemical compositions of polymeric surfaces after exposure to oxygen plasma and subsequent thermal annealing were determined by XPS. Changes in the chemical compositions of the surfaces were correlated with the wetting behavior of the surfaces. As it is well known, XPS is a very sensitive quantitative method for studying the surface atomic compositions of polymeric materials.

Chemical structures of PDMS which constitutes the main backbone of TPSC and that of PMMA are shown in Fig. 8. Also included

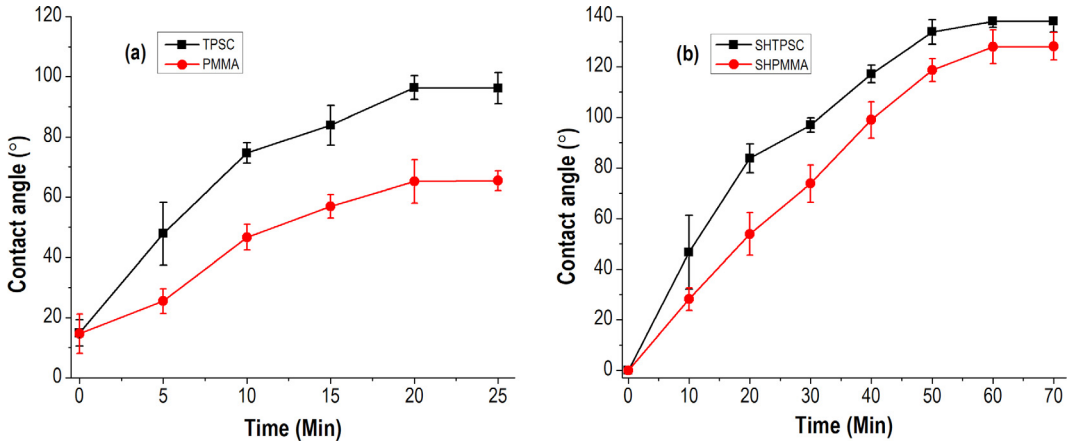

Fig. 7. Influence of annealing time on the recovery of hydrophobicity for (a) PMMA and TPSC surfaces (annealing temperature of 100 °C), and (b) SHPMMA and SHTPSC surfaces (annealing temperature of 150 °C).

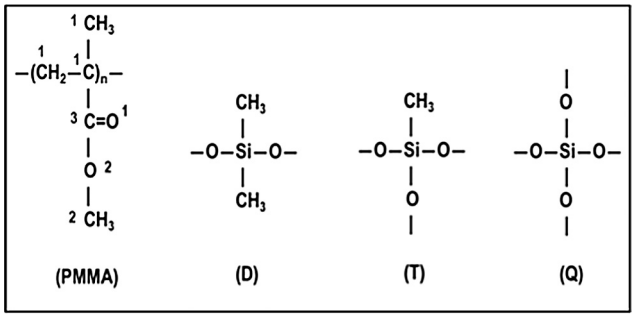

Fig. 8. Chemical structures of PMMA, dimethylsiloxane (D), methyltrisiloxane (T) and tetrasiloxane (Q).

in Fig. 8 are methyltrisiloxane (T) and tetrasiloxane (Q) units, which are generated by oxidation of dimethylsiloxane units (D). Various carbon and oxygen atoms in the PMMA unit are marked since they can be differentiated by XPS. In particular, binding energies (BEs) for 1s electrons of C1, C2 and C3 in PMMA are 284.5 eV, 286.2 eV and 288.5 eV respectively and for O1 and O2, BEs are 531.5 eV and 533.0 eV respectively. Similarly, BEs for 2p3/2 electrons of silicon atoms in D, T and Q are 102.0 eV, 102.7 eV and 103.2 eV respectively. A detailed survey of XPS spectra of PMMA, SHPMMA, TPSC and SHTPSC are provided in the supplementary information.

3.2.1. XPS studies on PMMA and SHPMMA

Deconvoluted regions of XPS spectra corresponding to C1s and O1s for fresh, oxidized and thermally annealed PMMA surfaces are reproduced in Figs. 9 and 10 respectively. In order to provide a complete picture of the chemical composition of surfaces investigated, relative concentration of each atom was calculated both with respect to all atoms present on the surface as well as with respect to the amount of atoms of the same chemical identity, e.g., ($C1/C_{total}$), where C_{total} = C1 + C2 + C3 (values presented within brackets in Table 2). As expected, upon oxidation, relative concentrations of C1 and C2 decrease due to the oxidation of the methyl and methoxy groups on PMMA [36]. On the other hand C3 increases since it is a highly oxidized carbonyl carbon. Upon thermal annealing at 100 °C for 20 min, atomic compositions very similar to fresh surfaces are obtained. This is attributed to dehydroxylation [37] and migration of low molecular weight species to the surface [38]. Similar behavior is observed in the XPS spectra of O1s peaks, where an increase in surface oxygen concentration upon oxidation and a decrease upon annealing is observed. Atomic percentages obtained from the XPS spectra together with the theoretical values for PMMA are given in Table 2.

Bulk composition of SHPMMA films consists of 9% by weight of PMMA and 91% by weight of hydrophobic fumed silica (HDK), which is mainly SiO_2. Therefore, XPS spectra of SHPMMA surfaces display very strong Si2p peaks at 103.2 eV and Si3p1/2 peak at 103.85 eV (with the spin-orbit splitting Δ = 0.65 eV), as shown in Fig. 11. A slight decrease in the concentration of Si is observed upon plasma oxidation or thermal annealing, as shown in Fig. 11b, c and Table 3; however, this change is negligible with respect to the high atomic concentration of Si. This is expected, since the majority of the film consists of already fully oxidized silica (SiO_2) agglomerates. Deconvoluted C1s region of the XPS spectra for SHPMMA surfaces are reproduced in Fig. 12 and the atomic percentages calculated from these spectra are provided in Table 3.

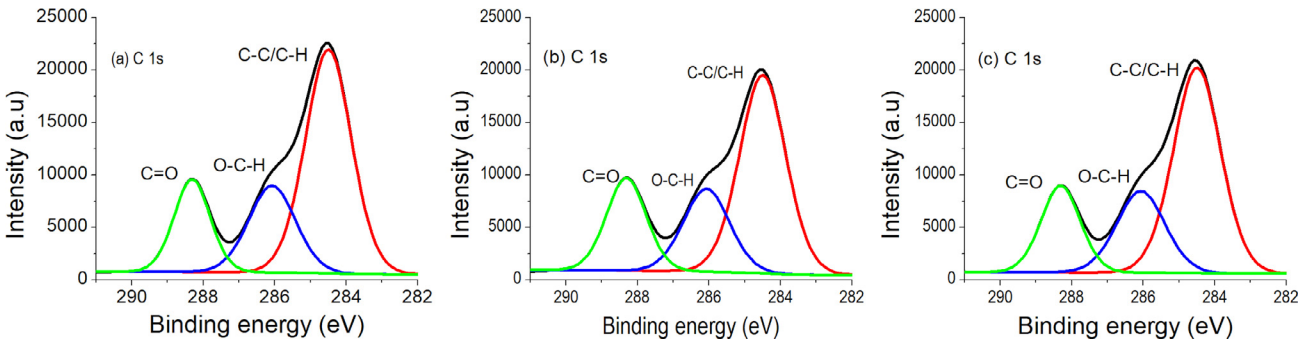

Fig. 9. Deconvoluted XPS peaks of C1s for; (a) fresh (b) oxidized and (c) thermally annealed PMMA surfaces. Black curves correspond to the raw XPS data.

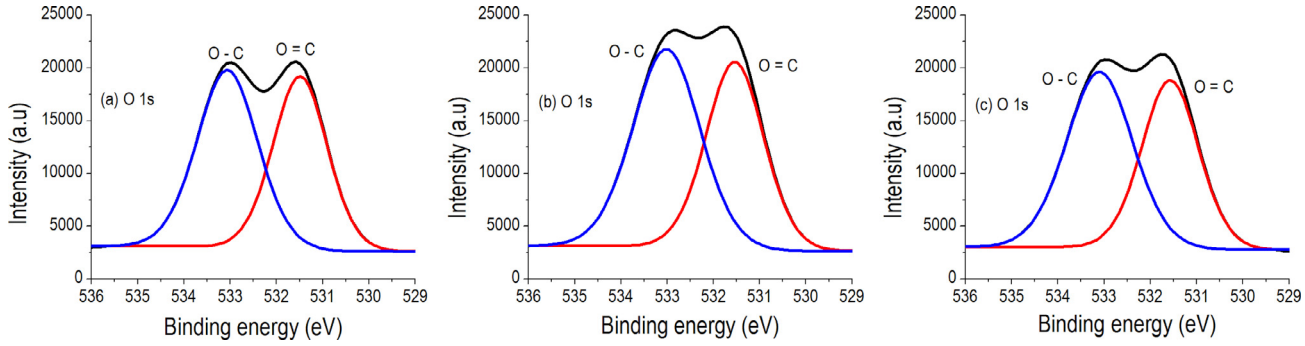

Fig. 10. Deconvoluted XPS peaks of O1s for; (a) fresh (b) oxidized and (c) thermally annealed PMMA surfaces. Black curves correspond to the raw XPS data.

Table 2
Atomic percentages of O1, O2, C1, C2, and C3 determined from the XPS spectra of fresh, plasma oxidized and thermally annealed PMMA surfaces together with the theoretical values. (O_{total} = O1 + O2, C_{total} = C1 + C2 + C3).

Atom	BE (eV)	Percent atomic composition			
		Theor. (%)	Fresh (%)	Oxidized (%)	Annealed (%)
O1 ($O1/O_{total}$)	531.5	14.3 (50)	12.4 (47)	14.2 (45)	12.8 (45)
O2 ($O2/O_{total}$)	533.0	14.3 (50)	14.2 (53)	17.4 (55)	15.5 (55)
C1 ($C1/C_{total}$)	284.5	42.8 (60)	42.7 (58)	37.6 (55)	40.8 (57)
C2 ($C2/C_{total}$)	286.2	14.3 (20)	16.9 (23)	15.7 (23)	16.6 (23)
C3 ($C3/C_{total}$)	288.5	14.3 (20)	13.8 (19)	15.1 (22)	14.3 (20)
O/C	–	0.40	0.36	0.44	0.39
O2/C1	–	0.33	0.33	0.46	0.38

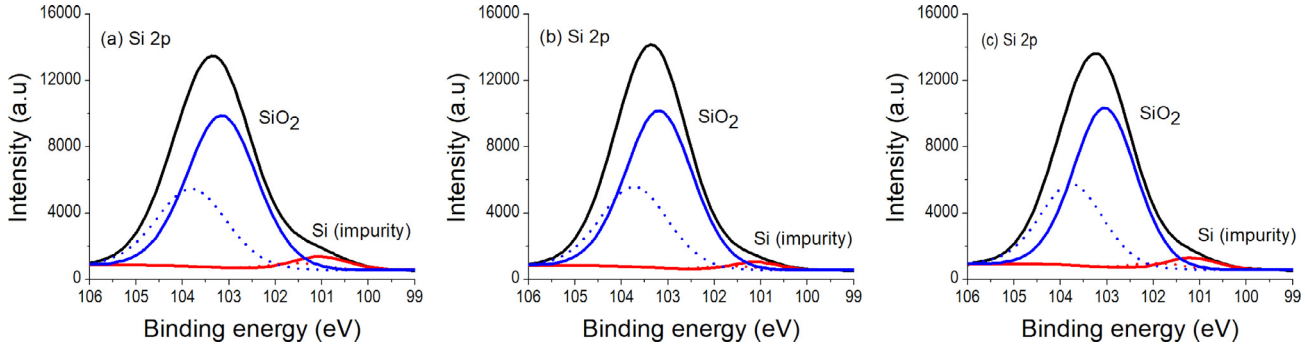

Fig. 11. Deconvoluted XPS peaks of Si2p for; (a) fresh (b) oxidized and (c) thermally annealed SHPMMA surfaces. Black curves correspond to the raw XPS data. Dotted lines correspond to spin orbit splitting.

Table 3
Atomic percentages of Si, O2, C1, C2, and C3 determined from the XPS spectra of fresh, plasma oxidized and thermally annealed SHPMMA surfaces together with the theoretical values. (C_{total} = C1 + C2 + C3).

Atom	BE (eV)	Percent atomic composition			
		Theor. (%)	Fresh (%)	Oxidized (%)	Annealed (%)
Si (Q)	103.2	30.3	30.9	28.8	27.8
O2	532.9	60.7	57.3	58.6	56.4
C1 ($C1/C_{total}$)	284.5	5.4 (60)	9.8 (83)	8.5 (67)	11.1 (70)
C2 ($C2/C_{total}$)	286.2	1.8 (20)	1.4 (12)	2.6 (12)	3.0 (19)
C3 ($C3/C_{total}$)	288.5	1.8 (20)	0.6 (5)	1.5 (21)	1.7 (11)

Main contribution of oxygen with BE of 532.9 eV comes from SiO_2 which is 10 times higher in concentration than PMMA in nanocomposites. In particular, the calculated oxygen content is 55.2% from silica and 5.5% from polymer. Thus, no major change in the concentration of O2 is observed upon plasma oxidation or thermal annealing. However, while the plasma-induced conversion of hydrophobic silica ($Si(CH_3)_2$) to hydrophilic moiety ($Si—O_x$) [39] might not cause a considerable increase in the surface oxygen concentration, it still contributes to the superhydrophilicity of the surface. Carbon spectra of SHPMMA look fairly similar to those of pure PMMA, where C1, C2 and C3 concentrations decrease slightly upon plasma exposure and increase after thermal annealing (Table 3), as expected.

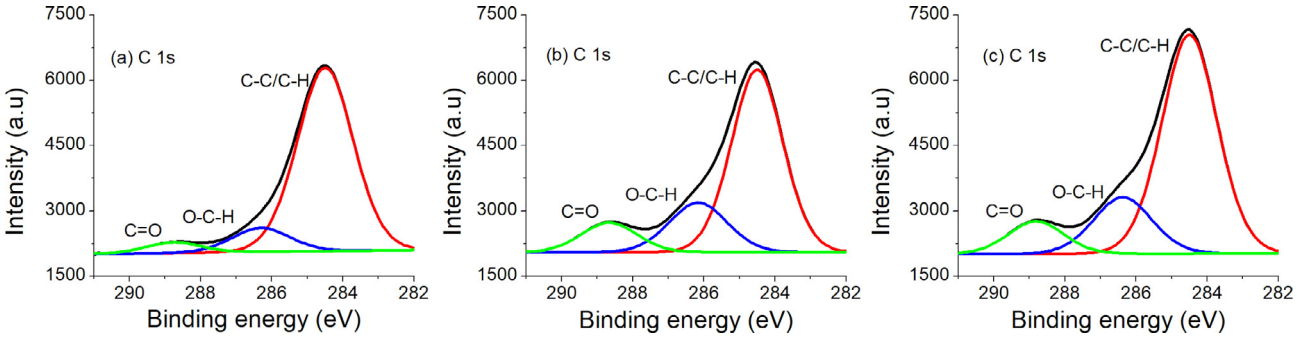

Fig. 12. Deconvoluted XPS peaks of C1s for; (a) fresh (b) oxidized and (c) thermally annealed SHPMMA surfaces. Black curves correspond to the raw XPS data.

3.2.2. XPS studies on TPSC and SHTPSC

TPSC is composed of alternating PDMS and urea segments. As shown in Fig. 13a, in the XPS spectrum of fresh TPSC film, Si2p3/2 peak of dimethylsiloxane unit (D) is at BE of 102.0 eV. When the film is exposed to plasma, oxidation of D units takes place. This results in splitting of the original Si peak into two peaks, representing D units and completely oxidized Q units, characterized by BE of 103.2 eV (Fig. 13b). Interestingly, no T unit formation is observed in the XPS data. After thermal annealing, peak of Q units with no hydrophobic methyl group decreases and peak of D units with two methyl groups increases. The restoration of the original chemical composition of the surface (Fig. 13c) can be clearly linked to the recovery of surface hydrophobicity. This recovery is mainly due to the migration of highly flexible PDMS segments with a lower surface energy from the bulk TPSC film to the film-air interface, replacing the oxidized Q layer. Atomic percentages determined from XPS spectra for fresh, plasma oxidized and thermally annealed TPSC surfaces together with the theoretical values are provided in Table 4.

XPS spectra of oxygen (Fig. 14) and carbon (Fig. 15) display characteristic trends similar to those observed for PMMA. As shown in Fig. 14, a single O1s peak with BE of 532.0 eV due to D units is observed in the fresh sample. After plasma oxidation, this peak shifts to a BE of 532.9 eV of Q units. As expected, after thermal recovery, relative surface concentration of D units increases and concentration of Q units decreases (Fig. 14c). Surface oxidation is further verified by a dramatic decrease in the carbon content upon plasma exposure (see Fig. 15). XPS spectrum of TPSC shows three carbon peaks; the most prominent one comes from the methyl groups on PDMS at BE of 284.5 eV, and a fairly small signal originates from the C—N and C═O groups present in urea at BE values of 286.0 eV and 288.8 eV, respectively. Upon oxidation, a dramatic decrease is observed in the amount of methyl carbons, which recover again upon thermal annealing. Due to low urea content

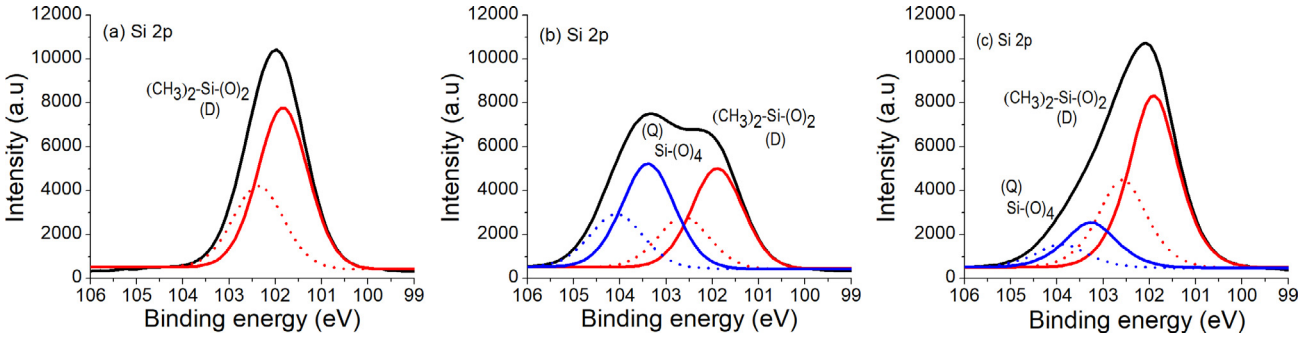

Fig. 13. Deconvoluted XPS peaks of Si2p for; (a) fresh (b) oxidized and (c) thermally annealed TPSC surfaces. Black curves correspond to the raw XPS data. Dotted lines correspond to spin orbit splitting.

Table 4
Atomic percentages of Si, O, C, and N determined from the XPS spectra of fresh, plasma oxidized and thermally annealed TPSC surfaces together with the theoretical values. (Si_{total} = Si_D + Si_Q, O_{total} = O_D + O_Q, C_{total} = C1 + C2 + C3).

Atom	Type	BE (eV)	Percent atomic composition			
			Theor. (%)	Fresh (%)	Oxidized (%)	Annealed (%)
Si_D (Si/Si_{total})	D	102.0	23.0 (100)	22.9 (100)	11.7 (49)	20.8 (78)
Si_Q (Si/Si_{total})	Q	103.2	– (–)	– (–)	12.4 (51)	5.7 (22)
O_D (O_D/O_{total})	D	532.0	23.8 (100)	22.2 (100)	0.8 (2)	26.8 (84)
O_Q (O_Q/O_{total})	Q	532.9	– (–)	– (–)	46.9 (98)	5.0 (16)
C1 ($C1/C_{total}$)	CH_3	284.5	49.4 (96)	47.3 (88)	22.1 (81)	38.7 (95)
C2 ($C2/C_{total}$)	C—N	286.0	1.5 (3)	5.1 (10)	3.3 (12)	2.1 (5)
C3 ($C3/C_{total}$)	C═O	288.8	0.8 (1)	1.1 (2)	1.8 (7)	– (–)
N	C—N	399.5	1.5	1.4	1.0	0.9
O/C	–	–	0.46	0.42	1.75	0.78
O/C1	–	–	0.48	0.47	2.16	0.82

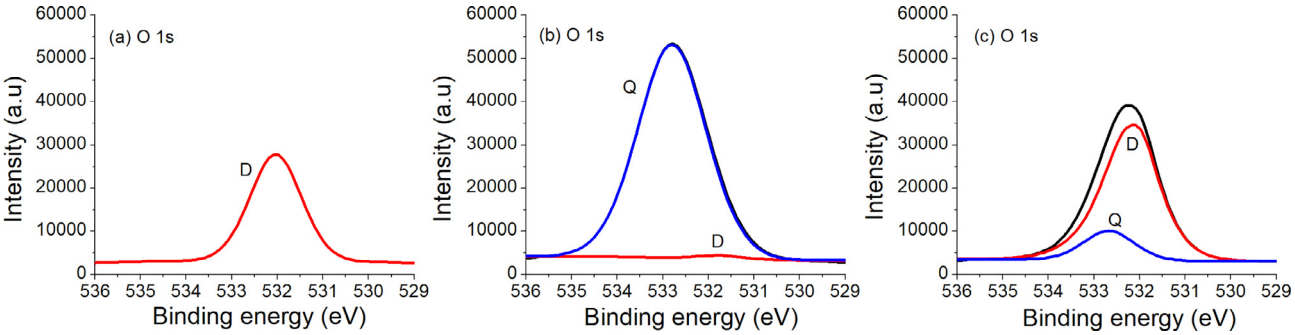

Fig. 14. Deconvoluted XPS peaks of O1s for; (a) fresh (b) oxidized and (c) thermally annealed TPSC surfaces. Black curves correspond to the raw XPS data.

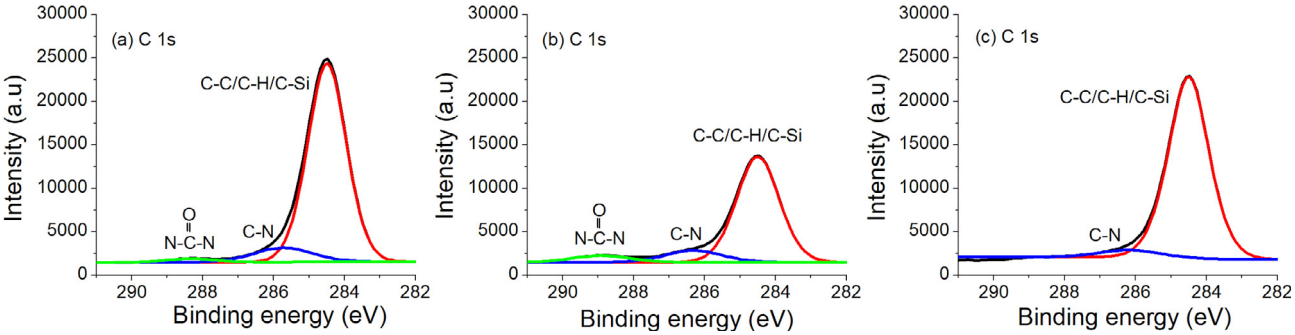

Fig. 15. Deconvoluted XPS peaks of C1s for; (a) fresh (b) oxidized and (c) thermally annealed TPSC surfaces. Black curves correspond to the raw XPS data.

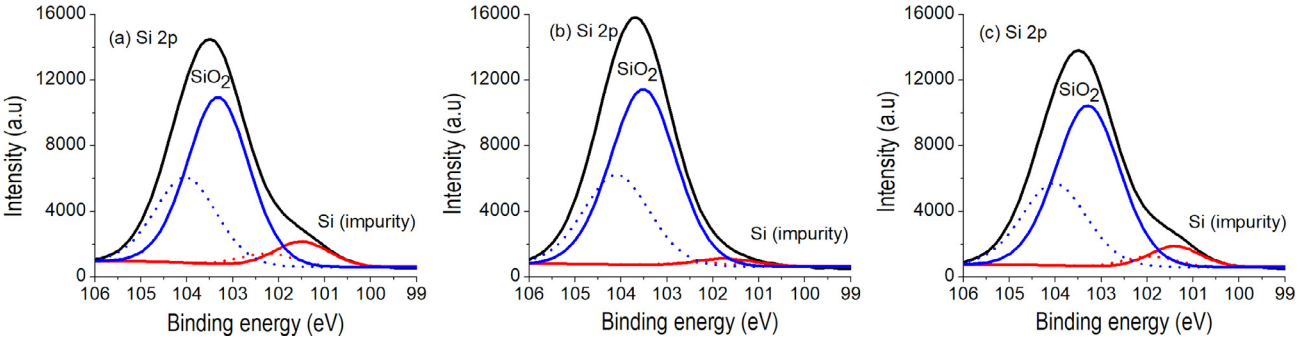

Fig. 16. Deconvoluted XPS peaks of Si2p for; (a) fresh (b) oxidized and (c) thermally annealed SHTPSC surfaces. Black curves correspond to the raw XPS data. Dotted lines correspond to spin orbit splitting.

in TPSC, change in urea carbons are fairly small as summarized in Table 4.

XPS spectra of SHTPSC silicon given in Fig. 16 show a dominant Si2p3/2 peak at a BE of 103.2 eV due to the presence of a large amount of fumed silica (SiO_2) in the film and a minor peak at BE of 101.4 eV due to PDMS backbone. Behavior similar to PMMA is observed for O1s peaks in XPS, where O1s from SiO_2 at a BE of 532.9 eV is dominant (not shown). Due to very small amount of TPSC binder in the film, XPS spectrum of carbon shows only one C1s peak coming from PDMS backbone at 284.5 eV (not shown). As summarized in Table 5, after plasma exposure atomic percentages calculated for Si and C atoms clearly show the conversion of D units to Q units. After thermal annealing, substantial recovery of D units is observed on the surface, which strongly correlates with the contact angle data discussed earlier.

3.3. Characterization of surface texture and topography before and after plasma treatment/thermal annealing

Detailed examination of surface texture and topography of all samples before and after plasma oxidation and after thermal annealing was carried out by SEM and WLI studies. Main aim of these studies was to assess if plasma oxidation and/or thermal annealing resulted in any change/damage of the surface texture, roughness or topography of the films. As shown in representative SEM images provided in Fig. 17, no noticeable changes were observed in the surface topography of any of the samples upon plasma oxidation and/or thermal annealing. Similar results were obtained by WLI, a non-contact optical technique, which is fairly precise in the determination of average values of surface roughness ranging from nanometer to millimeter scale. Average values of

Table 5
Atomic percentages of Si, O, C, and N determined from the XPS spectra of fresh, plasma oxidized and thermally annealed SHTPSC surfaces together with the theoretical values. ($Si_{total} = Si_D + Si_Q$, $C_{total} = C1 + C2 + C3$).

Atom	Type	BE (eV)	Percent atomic composition			
			Theor. (%)	Fresh (%)	Oxidized (%)	Annealed (%)
Si_D (Si_D/Si_{total})	D	101.4	4.8 (15)	3.9 (12)	1.4 (4)	3.1 (9)
Si_Q (Si_Q/Si_{total})	Q	103.2	27.9 (85)	28.7 (88)	30.6 (96)	29.7 (91)
O	Q	532.9	56.3	55.8	61.3	55.6
C1 ($C1/C_{total}$)	CH_3	284.5	10.7 (98)	11.4 (100)	4.6 (73)	11.4 (100)
C2 ($C2/C_{total}$)	C—N	286.0	0.1 (1)	– (–)	1.0 (16)	– (–)
C3 ($C3/C_{total}$)	C═O	288.8	0.1 (1)	– (–)	0.7 (11)	– (–)
N	N—C	–	0.1	0.2	0.4	0.2
O/C	–	–	5.14	4.89	9.73	4.88
O/C1	–	–	5.25	4.89	13.33	4.88

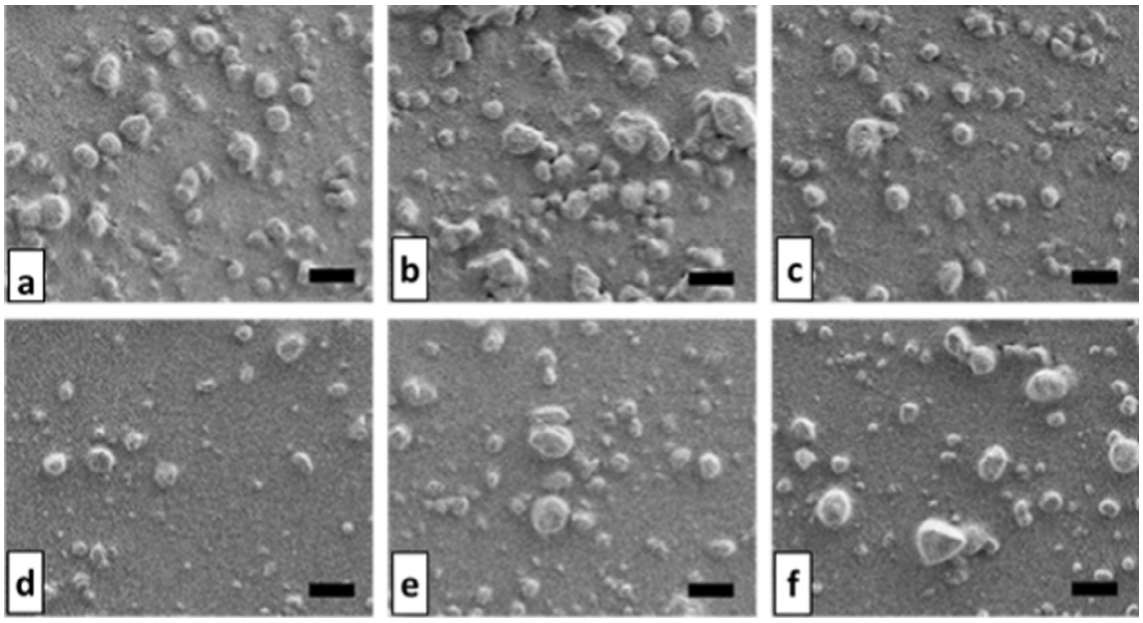

Fig. 17. SEM images of superhydrophobic surfaces; (a) fresh SHPMMA, (b) plasma oxidized SHPMMA, and (c) thermally annealed SHPMMA, (d) fresh SHTPSC, (e) plasma oxidized SHTPSC, and (f) thermally annealed SHTPSC. All scale bars are 10 μm.

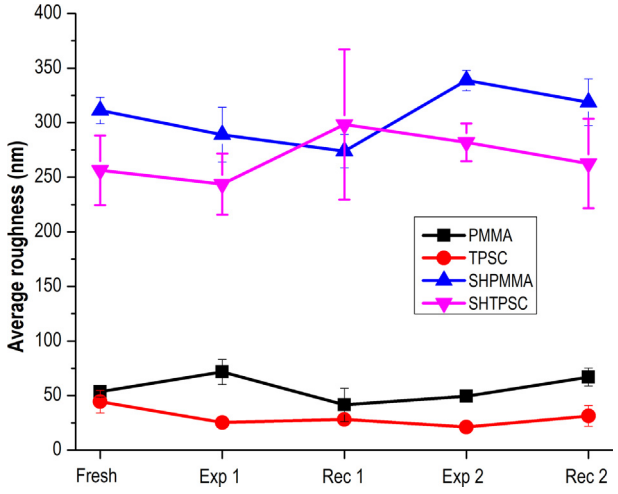

Fig. 18. Changes in the average values of roughness of polymer surfaces during two plasma exposure/thermal annealing cycles, determined by WLI.

surface roughness of the samples investigated in the course of two exposure/recovery cycles are plotted in Fig. 18. As seen in this figure, average roughness values do not show any significant change after completing individual treatment steps within the two cycles. Exemplary WLI images of investigated surfaces are provided in the Supporting Information.

3.4. Preparation of rewritable hydrophilic channels on hydrophobic TPSC surface

As a representative application of our developed surfaces with switchable wettability, we demonstrate preparation of reconfigurable hydrophilic tracks on a hydrophobic TPSC surface. These linear hydrophilic tracks shown in Fig. 19 were obtained by localized plasma activation of TPSC surfaces. To this end, we used a PDMS mask which defined the pattern layout consisting of a straight track (length: 15 mm, width: 1 mm) terminated by circular reservoirs (diameter: 3 mm) at each end. After placing the mask firmly on top of the TPSC film, the films were plasma-oxidized for 10 s at 1 W. Subsequently, the mask was removed and 15 μL of distilled water containing regular ink was placed on input reservoir. Upon deposition, water started flowing along the hydrophilic track until equilibrium was achieved in approximately one minute and water accumulated at the output reservoir. After completing the wetting experiment, the surface was dried and kept in an oven at 100 °C for 20 min for thermal annealing which recovered full surface hydrophobicity and erased the pattern. Plasma oxidation through

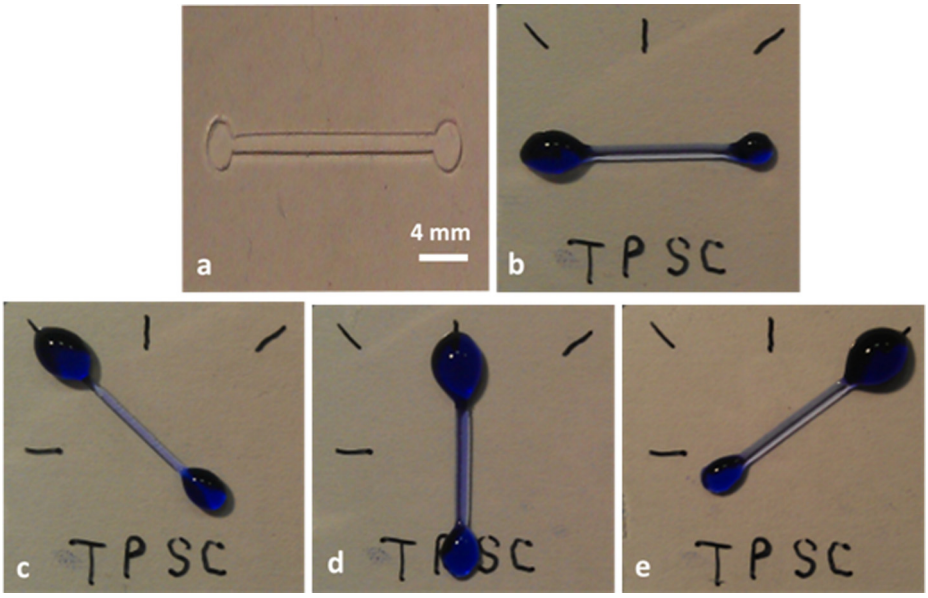

Fig. 19. Fabrication of erasable hydrophilic tracks on hydrophobic TPSC surfaces. (a) PDMS mask used to obtain hydrophilic patterns shown in (b – e). All patterns were created consecutively on the same hydrophobic TPSC film. Scale bar is identical for all samples.

the mask was then repeated three times with the mask placed over the surface with a 45° rotation relatively to its previous orientation. As shown in Fig. 19, in this way, water channels were obtained over the same TPSC surface at four different angles, after consecutive plasma oxidation and thermal recovery cycles. In all four consecutive channel writing/erasing experiments, water spread along the channels with a similar speed and the confinement of aqueous filaments to the plasma-treated TPSC region was comparably good. These results clearly demonstrate the possibility of fabricating completely recoverable microfluidic channels on TPSC surfaces.

4. Conclusions

Polymeric surfaces with wetting properties that can be repeatedly switched between superhydrophobic to superhydrophilic, using fairly simple processes of plasma oxidation and thermal annealing, have been demonstrated. For this purpose, we have adopted four polymer systems with inherently quite different surface properties; in particular, we used hydrophilic PMMA, hydrophobic TPSC and their superhydrophobic versions obtained by incorporation of hydrophobic fumed silica into the polymer matrix. For all studied polymer systems, we have observed reversible switching of surface wettability over many cycles of surface treatment. By determining optimum parameters for oxygen plasma exposure and thermal treatment, we have optimized the efficiency of the process in terms of speed of surface recovery, contrast of water contact angle between the two extremal wetting states, and number of useful recovery cycles. We have carried out comprehensive physical (SEM and WLI) and chemical (XPS) characterizations of the studied polymer surfaces in order to understand the principal phenomena taking place at the surfaces. SEM, WLI and XPS results have clearly shown that reversible switching of wetting characteristics took place solely due to chemical modification of polymer surfaces without any topographical alteration or deterioration. Using the above described simple processes for surface switching and a PDMS mask, we have achieved patterning of hydrophilic water channels on hydrophobic TPSC films by localized plasma oxidation. The channels could be erased by thermal annealing of the patterned sample in an oven at 100 °C for 20 min and could be successfully rewritten multiple times along an arbitrary direction, without any degradation of wetting contrast. Such reconfigurable and patternable surfaces hold promise for applications in surface microfluidics, droplet microfluidics and optofluidics, in which chemical or biological reagents encapsulated in droplets or even light confined in a liquid can be guided with ease and flexibility.

Acknowledgement

Z. Rashid thanks HEC Pakistan for Ph.D. scholarship. The authors thank Koç University, Surface Science and Technology Center (KUYTAM) for providing reliable state of the art equipment to carry out experiments and measurements.

Appendix A. Supplementary material

Supplementary data associated with this article can be found, in the online version, at https://doi.org/10.1016/j.apsusc.2018.02.089.

References

[1] W. Sun, S. Zhou, B. You, L. Wu, A facile method for the fabrication of superhydrophobic films with multiresponsive and reversibly tunable wettability, J. Mater. Chem. A Mater. Energy Sustain. 1 (2013) 3146.
[2] G. Petroffe, C. Wang, X. Sallenave, G. Sini, F. Goubard, S. Péralta, Fast and reversible photo-responsive wettability on TiO_2 based hybrid surfaces, J. Mater. Chem. A Mater. Energy Sustain. 3 (2015) 11533–11542.
[3] N.J. Shirtcliffe, G. McHale, M.I. Newton, C.C. Perry, P. Roach, Porous materials show superhydrophobic to superhydrophilic switching, Chem. Commun. 3135 (2005).
[4] S. Minko, M. Müller, M. Motornov, M. Nitschke, K. Grundke, M. Stamm, Two-level structured self-adaptive surfaces with reversibly tunable properties, J. Am. Chem. Soc. 125 (2003) 3896–3900.
[5] T.N. Krupenkin, J. Ashley Taylor, E.N. Wang, P. Kolodner, M. Hodes, T.R. Salamon, Reversible wetting–dewetting transitions on electrically tunable superhydrophobic nanostructured surfaces, Langmuir. 23 (2007) 9128–9133.
[6] H.S. Lim, J.T. Han, D. Kwak, M. Jin, K. Cho, Photoreversibly switchable superhydrophobic surface with erasable and rewritable pattern, J. Am. Chem. Soc. 128 (2006) 14458–14459.
[7] C.-H. Xue, Z.-D. Zhang, J. Zhang, S.-T. Jia, Lasting and self-healing superhydrophobic surfaces by coating of polystyrene/SiO_2 nanoparticles and polydimethylsiloxane, J. Mater. Chem. A Mater. Energy Sustain. 2 (2014) 15001–15007.
[8] K. Tsougeni, N. Vourdas, A. Tserepi, E. Gogolides, C. Cardinaud, Mechanisms of oxygen plasma nanotexturing of organic polymer surfaces: from stable super hydrophilic to super hydrophobic surfaces, Langmuir. 25 (2009) 11748–11759.

[9] K.E. Herold, A. Rasooly, Lab on a Chip Technology: Fabrication and microfluidics, Horizon Scientific Press, 2009.
[10] C. Jin, R. Yan, J. Huang, Cellulose substance with reversible photo-responsive wettability by surface modification, J. Mater. Chem. 21 (2011) 17519.
[11] J.T. Han, X. Xu, K. Cho, Diverse access to artificial superhydrophobic surfaces using block copolymers, Langmuir. 21 (2005) 6662–6665.
[12] Y.Y. Yan, N. Gao, W. Barthlott, Mimicking natural superhydrophobic surfaces and grasping the wetting process: a review on recent progress in preparing superhydrophobic surfaces, Adv. Colloid Interface Sci. 169 (2011) 80–105.
[13] H.Y. Erbil, A.L. Demirel, Y. Avci, O. Mert, Transformation of a simple plastic into a superhydrophobic surface, Science. 299 (2003) 1377–1380.
[14] K. Acatay, E. Simsek, C. Ow-Yang, Y.Z. Menceloglu, Tunable, superhydrophobically stable polymeric surfaces by electrospinning, Angew. Chem. Int. Ed Engl. 43 (2004) 5210–5213.
[15] D. Öner, T.J. McCarthy, Ultrahydrophobic Surfaces Effects of Topography Length Scales on Wettability, Langmuir 16 (2000) 7777–7782.
[16] C.K. Söz, E. Yilgör, I. Yilgör, Influence of the coating method on the formation of superhydrophobic silicone–urea surfaces modified with fumed silica nanoparticles, Prog. Org. Coat. 84 (2015) 143–152.
[17] M. Sun, C. Luo, L. Xu, H. Ji, Q. Ouyang, D. Yu, Y. Chen, Artificial lotus leaf by nanocasting, Langmuir. 21 (2005) 8978–8981.
[18] N.J. Shirtcliffe, G. McHale, M.I. Newton, C.C. Perry, Intrinsically superhydrophobic organosilica Sol−Gel foams, Langmuir. 19 (2003) 5626–5631.
[19] I. Yilgor, S. Bilgin, M. Isik, E. Yilgor, Facile preparation of superhydrophobic polymer surfaces, Polymer 53 (2012) 1180–1188.
[20] P.N. Manoudis, I. Karapanagiotis, A. Tsakalof, I. Zuburtikudis, C. Panayiotou, Superhydrophobic composite films produced on various substrates, Langmuir 24 (2008) 11225–11232.
[21] X. Tang, T. Wang, F. Yu, X. Zhang, Q. Zhu, L. Pang, G. Zhang, M. Pei, Simple, robust and large-scale fabrication of superhydrophobic surfaces based on silica/polymer composites, RSC Adv. 3 (2013) 25670.
[22] X. Tang, F. Yu, W. Guo, T. Wang, Q. Zhang, Q. Zhu, X. Zhang, M. Pei, A facile procedure to fabricate nano calcium carbonate–polymer-based superhydrophobic surfaces, New J. Chem. 38 (2014) 2245–2249.
[23] P. Roach, N.J. Shirtcliffe, M.I. Newton, Progess in superhydrophobic surface development, Soft Matter. 4 (2008) 224–240.
[24] K. Liu, L. Jiang, Bio-inspired self-cleaning surfaces, Annu. Rev. Mater. Res. 42 (2012) 231–263.
[25] S. Subhash Latthe, S.S. Latthe, A.B. Gurav, C.S. Maruti, R.S. Vhatkar, Recent progress in preparation of superhydrophobic surfaces: a review, J. Surface Eng. Mater. Adv. Technol. 02 (2012) 76–94.
[26] Z. Guo, W. Liu, B.-L. Su, Superhydrophobic surfaces: from natural to biomimetic to functional, J. Colloid Interface Sci. 353 (2011) 335–355.
[27] L. Hong, T. Pan, Surface microfluidics fabricated by photopatternable superhydrophobic nanocomposite, Microfluid. Nanofluidics. 10 (2010) 991–997.
[28] S. Xing, R.S. Harake, T. Pan, Droplet-driven transports on superhydrophobic-patterned surface microfluidics, Lab Chip. 11 (2011) 3642–3648.
[29] C.K. Söz, E. Yilgör, I. Yilgör, Simple processes for the preparation of superhydrophobic polymer surfaces, Polymer. 99 (2016) 580–593.
[30] A. Jonáš, B. Yalizay, S. Akturk, A. Kiraz, Free-standing optofluidic waveguides formed on patterned superhydrophobic surfaces, Appl. Phys. Lett. 104 (2014) 091123.
[31] R. de Ruiter, A.M. Pit, V.M. de Oliveira, M.H.G. Duits, D. van den Ende, F. Mugele, Electrostatic potential wells for on-demand drop manipulation in microchannels, Lab Chip. 14 (2014) 883–891.
[32] Z. Rashid, U.C. Coşkun, Y. Morova, B. Morova, A.A. Bozkurt, A. Erten, A. Jonáš, S. Aktürk, A. Kiraz, Guiding of emulsion droplets in microfluidic chips along shallow tracks defined by laser ablation, Microfluid. Nanofluidics. 21 (2017), https://doi.org/10.1007/s10404-017-1997-1.
[33] A.F. Stalder, T. Melchior, M. Müller, D. Sage, T. Blu, M. Unser, Low-bond axisymmetric drop shape analysis for surface tension and contact angle measurements of sessile drops, Colloids Surf. A Physicochem. Eng. Asp. 364 (2010) 72–81.
[34] Z. Xu, V. Shilpiekandula, K. Youcef-toumi, S.F. Yoon, White-light scanning interferometer for absolute nano-scale gap thickness measurement, Opt. Express. 17 (2009) 15104–15117.
[35] E. Yilgör, E. Burgaz, E. Yurtsever, I. Yilgör, Comparison of hydrogen bonding in polydimethylsiloxane and polyether based urethane and urea copolymers, Polymer. 41 (2000) 849–857.
[36] G. Slaughter, B. Stevens, A cost-effective two-step method for enhancing the hydrophilicity of PDMS surfaces, Biochip J. 8 (2014) 28–34.
[37] V.Y. Davydov, V.Ya. Davydov, A.V. Kiselev, L.T. Zhuravlev, Study of the surface and bulk hydroxyl groups of silica by infra-red spectra and D2O-exchange, Transact. Faraday Soc. 60 (1964) 2254.
[38] H. Hillborg, N. Tomczak, A. Olàh, H. Schönherr, G.J. Vancso, Nanoscale hydrophobic recovery: a chemical force microscopy study of UV/ozone-treated cross-linked poly(dimethylsiloxane), Langmuir. 20 (2004) 785–794.
[39] H. Hillborg, N. Tomczak, A. Olàh, H. Schönherr, G.J. Vancso, Hydrophilization of silicone-urea copolymer surfaces by UV/ozone: Influence of PDMS molecular weight on surface oxidation and hydrophobic recovery, Polymer. 54 (2013) 6665–6675.